Inorganic Chemistry

Article

pubs.acs.org/IC

Role of Entropy and Autosolvation in Dimerization and Complexation of C_{60} by Zn_7 Metallocavitands

Peter D. Frischmann,[†] S. Hessam M. Mehr,[†] Brian O. Patrick,[†] Francesco Lelj,*[,‡] and Mark J. MacLachlan*[,†]

[†]Department of Chemistry, University of British Columbia, 2036 Main Mall, Vancouver, British Columbia, Canada V6T 1Z1

[‡]La.M.I. and LaSCAMM INSTM Sezione Basilicata, Dipartimento di Chimica, Università della Basilicata, via dell'Ateneo Lucano 10, 85100 Potenza, Italy

Supporting Information

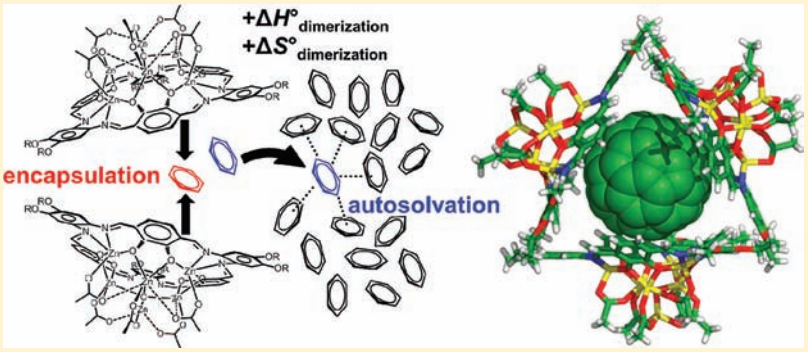

ABSTRACT: The supramolecular chemistry of bowl-shaped heptazinc metallocavitands templated by Schiff base macrocycles has been investigated. Dimerization thermodynamics were probed by ^{1}H NMR spectroscopy in benzene-d_6, toluene-d_8, and *p*-xylene-d_{10} and revealed the process to be entropy-driven and enthalpy-opposed in each solvent. Trends in the experimentally determined enthalpy and entropy values are related to the thermodynamics of solvent autosolvation, solvent molecules being released from the monomeric metallocavitand cavity into the bulk solvent upon dimerization. The relationship established between experimentally measured dimerization thermodynamics and autosolvation data successfully predicts the absence of dimerization in CH_2Cl_2 and $CHCl_3$ and was used to estimate the number of solvent molecules interacting with the monomeric metallocavitand in solution. Host–guest interactions between heptazinc metallocavitands and fullerene C_{60} have also been investigated. Interestingly, metallocavitand-C_{60} interactions are only observed in solvents that facilitate entropy-driven dimerization suggesting entropy and solvent autosolvation may be important in explaining concave-convex interactions.

INTRODUCTION

Organic cavitands such as calixarenes, resorcinarenes, and cyclotriveratrylenes have played a central role in the development of supramolecular chemistry.[1] Because of the quintessential bowl shape of cavitands, small guest molecules often bind noncovalently inside the cavity giving rise to applications such as small molecule sensing,[2] medical imaging,[3] reactive intermediate trapping,[4] controlling photochemical reactivity,[5] and host–guest catalysis.[6] Selective guest encapsulation is achieved by matching shape and electronic interactions between the concave cavitand and convex guest molecules. Complementary host–guest or host–host interactions may also drive self-assembly of cavitands into noncovalent dimers,[7] polyhedra,[8] or polymers.[9]

One strategy for expanding the breadth of cavitand host–guest chemistry involves incorporating coordinatively unsaturated transition metals into traditional organic cavitands. Cavitand coordination complexes may potentially exhibit both the selective guest recognition of organic supramolecular chemistry and catalytic, magnetic, and optical properties of metals.[10,11] Recently, Matt et al. reported robust Ni complexes of calix[4]arenes with triarylphosphine functionalized upper rims that catalyze Kumada–Tamao–Corriu cross-coupling reactions through a proposed [Ni(π-ArX)(calix-phosphine)] supramolecular host–guest intermediate.[12] Richeter and Rebek have modified a deep resorcin[4]arene to include a zinc(II) salphen (*N*,*N*′-bis(salicylidine)-*o*-phenylenediimine) unit near the periphery of the cavitand.[13] This complex binds ammonium functional groups in the cavity and catalyzes reactions at the metal active site.[14] Acting harmoniously, the cavity sorts substrates by size and electrostatics while locking a portion of the substrate in close proximity to the Lewis acidic zinc(II) salphen center. Specifically, this metalated cavitand system catalyzes the esterification of choline to acetylcholine and catalytically hydrolyzes certain carbonates. Enzyme-like selec-

Received: September 20, 2011
Published: February 29, 2012

   dx.doi.org/10.1021/ic202049t | *Inorg. Chem.* 2012, 51, 3443–3453

Scheme 1. Synthesis of Heptazinc Metallocavitands 2a–c from [3 + 3] Schiff Base Macrocycles 1a–c

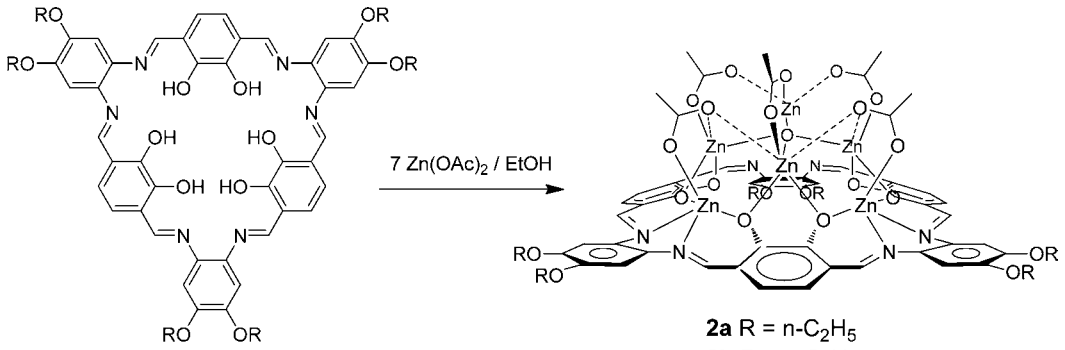

1a R = n-C_2H_5
1b R = n-C_6H_{13}
1c R = n-C_8H_{17}

2a R = n-C_2H_5
2b R = n-C_6H_{13}
2c R = n-C_8H_{17}

tivity and rate enhancements are achieved because of synergy between the cavity and the metal active site.[15] Notably, in cavitand coordination complexes the metal ion(s) are coordinated at the rim or center of the organic cavitand and have little effect on the intrinsic curvature of the host molecule.

Our research efforts have focused on developing metal-containing cavitands using a fundamentally different approach. While the majority of bowl-shaped coordination complexes rely upon traditional organic cavitands for curvature, our system begins with a nearly planar [3 + 3] Schiff base macrocycle[16] that adopts a bowl shape upon coordination of seven metal ions as outlined in Scheme 1. We have previously suggested the term *metallocavitand* be used to describe these new multimetallic complexes where metal coordination is necessary for cavity formation.[17] Like traditional organic cavitands, metallocavitands exhibit a wealth of interesting supramolecular chemistry such as host–guest binding,[18] small molecule sensing,[19] unusual reactivity of confined guests,[20] and self-association.[21] Another developing advantage of metallocavitands is that multiple metal centers are often held in close proximity, potentially yielding multimetallic catalysts.[22]

Recently we reported heptacadmium metallocavitands templated by macrocycles **1a–c** that exhibit entropy-driven dimerization, dynamic ligand exchange, and have an unusual central μ_3-OH ligand capable of H-bonding with encapsulated guest molecules.[23] The cadmium carboxylate cluster coordinated above the plane of the macrocycle closely resembles a $[Cd_4(OAc)_9(\mu_3\text{-}OH)]^{2-}$ secondary building unit.[24] Capsules of these cadmium metallocavitands with two encapsulated dimethylformamide (DMF) guest molecules exhibit exceptionally high packing coefficients (0.80). This dense packing is attributed to simultaneous metal–ligand and H-bonding synergy between host and guest inside the capsule and demonstrates the emergence of interesting properties when metal ions are incorporated into the cavity of host molecules.

Zinc complexes are far more appealing for applications than cadmium because of the enhanced Lewis acidity and lower toxicity of zinc compared to cadmium. In particular, zinc salphen complexes have been utilized in molecular recognition and sensing,[25] catalysis,[26] and self-assembly of complex architectures.[27,28] Metallocavitands **2a–c** may be described as tris-zinc salphens with a basic zinc acetate cluster, $Zn_4O(OAc)_6$, coordinated in the center of the macrocycle.[29] Ohshima and co-workers replaced the acetato ligands of basic zinc acetate with trifluoroacetato ligands to yield a powerful catalyst capable of selectively acylating alcohols in the presence of amines.[30] Basic zinc acetate (carboxylate) clusters are also a common secondary building unit in metal–organic frameworks.[31] Schiff base macrocycles **1a–c** template the formation of basic zinc acetate in a stepwise manner to form metallocavitands **2a–c**.[32] The basic metal–ligand linkage within these clusters is similar to a metallacoronate.[33] Introduction of 1 equiv of $La(OAc)_3$ results in transmetalation of the entire basic zinc acetate cluster and formation of a new heterometallic metallocavitand.[29b,34] Although much has been discovered about the structural features and reactivity of **2a–c**, until now little has been known about their supramolecular chemistry.

In this article, dimerization of heptazinc metallocavitands is investigated in detail by single-crystal X-ray diffraction (SCXRD), variable-temperature and variable-concentration ^{1}H NMR spectroscopy, and density functional theory (DFT) calculations. Interestingly, dimerization of **2b–c** is entropy-driven in aromatic solvents unlike most cavitands where dimerization is often an enthalpy-driven process facilitated by favorable H-bonding, electrostatic, or van der Waals interactions. A linear relationship between the experimentally derived dimerization thermodynamics and solvent autosolvation thermodynamics is observed that suggests dimerization of Zn_7 metallocavitands is controlled by solvent autosolvation. This relationship also provides insight into the host–guest interactions between solvent molecules and monomeric metallocavitands.

DFT geometry optimizations were performed to verify the solid-state $Zn_4O(OAc)_6$ cluster geometry and to gain insight into the solution stability of the cluster. These calculations also confirmed the μ_4-oxo cluster configuration is favored over the μ_3-hydroxo configuration previously observed in similar heptacadmium metallocavitands. Finally, the host–guest interaction of metallocavitands with C_{60} fullerene is discussed with implications that entropy and autosolvation effects may control Zn_7 metallocavitand-C_{60} complexation.

EXPERIMENTAL SECTION

Methods. Macrocycles **1a–c**[16a,b] and metallocavitands **2a–c**[23b,29a] were prepared by literature procedures. C_{60} (99% purity) was purchased from MER Corporation and used without any further purification. ^{1}H NMR spectra were recorded on a Bruker AV-400 inverse probe spectrometer and were calibrated to the residual protonated solvent at δ 7.27, 7.16, 5.32, 2.09, and 2.21 for $CDCl_3$, C_6D_6, CD_2Cl_2, toluene-d_8, and *p*-xylene-d_{10}, respectively.

dx.doi.org/10.1021/ic202049t | *Inorg. Chem.* 2012, 51, 3443–3453

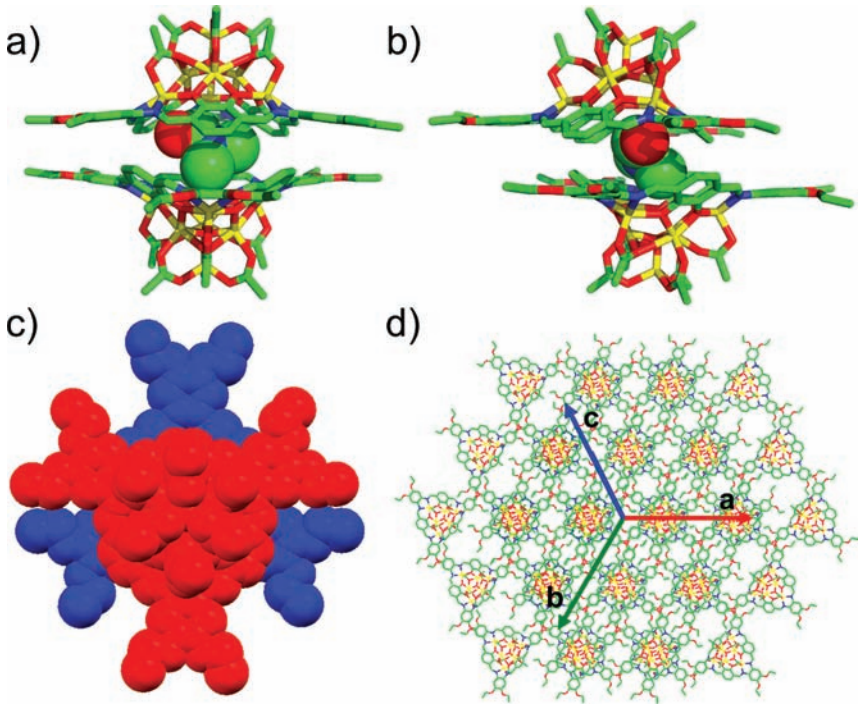

Figure 1. Solid-state structure of **2a** highlighting the dimer and encapsulated DMF. (a) Side-on view. (b) Side-on view rotated 90° from (a). (c) Top-down view where the capsule halves are colored red and blue. (d) Long-range hexagonal packing of the capsules. Hydrogen atoms have been omitted for clarity. (C = green, N = blue, O = red, Zn = yellow).

Single-Crystal X-ray Diffraction. The SCXRD experiment was conducted on a Bruker APEX DUO diffractometer with $Mo_{K\alpha}$ radiation. The structure was solved by direct methods with SIR1997[35] and refined with SHELXL-97.[36] The material crystallizes with approximately 10 molecules of DMF (C_3H_7NO) in the asymmetric unit. Three of these molecules were disordered and were modeled in two orientations with site-occupancies summing to one. There was one region of unresolved electron density that could not be properly modeled; therefore, the PLATON/SQUEEZE[37] program was used to generate a data set "free" of solvent at that site. The total amount of electron density removed from the model was 128 e^-, or 64 e^- per asymmetric unit, which is approximately 1.5 DMF molecules. Of the remaining solvent molecules, eight are in general positions in the asymmetric unit, while one resides disordered (with 0.5 occupancy) about an inversion center occupying the space inside the dimer. The final empirical formula consists of the macrocycle and 10 DMF molecules. All non-hydrogen atoms were refined anisotropically. All hydrogen atoms were placed in calculated positions. A capsule void space of 118 Å^3 was calculated with the PLATON/SQUEEZE program. See the Supporting Information, Figure 14 for a thermal ellipsoid plot. Data for **2a**: $C_{96}H_{136}N_{16}O_{35}Zn_7$, M_w = 2531.80 g mol^{-1}, red irregular (0.32 × 0.15 × 0.05 mm^3), triclinic, space group $P\bar{1}$, a = 16.669(3) Å, b = 19.244(4) Å, c = 20.811(6) Å, α = 97.611(5)°, β = 106.637(5)°, γ = 115.009(3)°, V = 5544(2) Å^3, Z = 2, ρ_{calcd} = 1.517 g cm^{-3}, F_{000} = 2628, $Mo_{K\alpha}$ radiation, λ = 0.71073 Å, T = 90.0(1) K, $2\theta_{max}$ = 51.4°, 110860 reflections collected, 20929 were unique (R_{int} = 0.059). Final GoF = 1.133, $R1$ = 0.0640, $wR2$ = 0.1913, R indices based on 14357 reflections with $I > 2\sigma(I)$.

Variable-Temperature and Variable-Concentration ^{1}H NMR Spectroscopy. Owing to low solubility of **2b** and **2c** in aromatic solvents, the concentration range was limited (0.1 to 5.0 mmol L^{-1}). A standard 5.0 mmol L^{-1} solution was first prepared by dissolving (with heating) 0.0050 mmol of metallocavitand in 1.0 mL of the deuterated solvent of choice. Except for the 5.0 mmol L^{-1} samples, NMR tubes were primed with 500 μL of selected deuterated solvent, and the standard solution was then added via syringe to achieve the desired concentrations. The concentration and temperature dependence of the imine resonance was measured in CD_2Cl_2, C_6D_6, toluene-d_8, and p-xylene-d_{10} for **2c** and only in toluene-d_8 for **2b**. The data were treated with the following least-squares curve-fitting equation (monomer–dimer equilibrium model) to find the dimerization constant, K_{dim}:[38]

$$(\delta - \delta_m) = (\delta_d - \delta_m)\left(1 + \frac{1 - \sqrt{8K_{dim}C_T + 1}}{4K_{dim}C_T}\right)$$

In this equation, δ is the experimentally determined chemical shift, δ_m is the absolute chemical shift of the monomer, δ_d is the absolute chemical shift of the dimer, and C_T is the total concentration of monomer in the absence of dimer.

Computational Details. To support the experimental results, DFT calculations were performed with Gaussian03 (revision D02) and Gaussian09 (revision A2) packages.[39] To reduce computational time, peripheral alkoxy chains on the phenylenediimine units were replaced by hydroxyl groups. DFT was applied using both pure PBE[40] and the hybrid B98[41] or PBE1PBE[42] xc functionals. Preliminary geometry optimizations were performed using the 3-21 g basis set.[43] All final results were performed with the Dunning/Huzinaga valence double-ζ (D95) basis sets,[44] adding a set of polarization functions to the same basis set in case of C, N, and O. The Stuttgart/Dresden ECP basis set[45] and pseudopotential (SDD) including relativistic effects were used for Zn atoms. Further computations using the M06[46] xc functional were undertaken to evaluate the weak intermolecular interaction in the case of $CHCl_3$ or benzene and the metallocavitand. Basis set superimposition error (BSSE)[47,48] contributions to the interaction enthalpies have been corrected by means of the Boys and Bernardi counterpoise (CP) approach. These corrections ranged from 28% to 39% of the value of the interaction enthalpy.

Default gradient and displacement thresholds were used for the geometry optimization convergence criteria. To confirm that the obtained geometries are relative minima of the molecular energy, analytical computation of the Hessian matrix with respect to the nuclear coordinates at the same level of theory was performed.

Time dependent DFT (TD-DFT)[49] calculations of the UV–vis spectrum were performed at the D95(d)/SDD/PBE1PBE1 level of theory. Structures and the Kohn–Sham orbitals were drawn with the programs GaussView3.0 and Molekel4.3.[50]

dx.doi.org/10.1021/ic202049t | Inorg. Chem. 2012, 51, 3443–3453

RESULTS AND DISCUSSION

Single-Crystal X-ray Diffraction. Slow evaporation of a solution of **2a** in DMF yielded deep red single-crystals of suitable quality for X-ray diffraction analysis.[51] In DMF, metallocavitand **2a** crystallizes with two molecules in a face-to-face orientation in which one bowl is twisted 60° and shifted slightly off-center, forming a C_{2h} symmetric capsule (nearly D_{3d} symmetry) in the solid state (Figure 1). There are 50 intermolecular atom-to-atom interactions less than the van der Waals distances (+0.2 Å) between the two molecules of **2a** that make up the capsule. One DMF molecule is found inside the capsule disordered about an inversion center. The oxygen atom of the encapsulated DMF molecule points directly at a zinc ion bound in a salphen pocket of the metallocavitand and exhibits a host–guest Zn–O (DMF) distance of 2.59 Å. A SQUEEZE calculation of the dimer with the encapsulated DMF removed indicated that within the capsule is 118 Å^3 of void space, thus yielding a packing coefficient (guest volume/host void space volume) of 0.68. This number is higher than the optimal solution packing coefficient predicted by the empirical "55 ± 9% rule" developed for host–guest chemistry by Mecozzi and Rebek.[52] A caveat for the observed deviation is the synergy of both van der Waals forces and weak metal–ligand interactions between host and guest inside capsules of **2a** that permit denser packing of the guest.[53] Only monomeric metallocavitands were observed by SCXRD analysis conducted on crystals of **2a** grown from DMSO in which DMSO is coordinated inside the cavity of **2a** via a Zn–O (DMSO) bond.[29a]

Monomeric metallocavitand **2a** is a trimetalated macrocycle with a $Zn_4O(OAc)_6$ cluster coordinated in the center, above the plane formed by the catechol oxygen atoms in the interior of the macrocycle. To accommodate the $Zn_4O(OAc)_6$ cluster, the trimetalated macrocycle adopts a concave conformation. Figure 2 depicts the geometry of monomeric **2a** and highlights the $Zn_4(\mu_4\text{-O})$ cluster. The molecular geometry of **2a**, revealed by SCXRD analysis, is very similar to previous SCXRD experiments on heptazinc metallocavitands that have been discussed in detail.[32b]

Structurally similar heptacadmium metallocavitands have a central μ_3-hydroxo ligand instead of a μ_4-oxo ligand that imparts interesting host–guest properties on the system.[23a] To determine if heptazinc metallocavitands **2a–c** may exist in equilibrium with a similar μ_3-hydroxo cluster configuration, a heptazinc metallocavitand with a central μ_3-hydroxo ligand was optimized by DFT computations, and the thermodynamic stability of the cluster has been assessed.

DFT Evaluation of the μ_4-oxo and μ_3-hydroxo Equilibrium and UV–visible Spectrum. Heptacadmium metallocavitands analogous to **2a–c** are stabilized by a μ_3-hydroxo ligand in the core of the metallocavitand cluster and not a μ_4-oxo ligand. To evaluate whether the μ_4-oxo ligand, observed for **2a** by SCXRD, is thermodynamically favored over a μ_3-hydroxo ligand and not just a solid-state phenomenon, we performed DFT calculations. Computational effort was minimized by substituting peripheral alkyl groups with protons (R = H).

To preserve the total number of electrons, the computations are based on the equilibrium shown in Scheme 2 where the nonbonded water molecule is in van der Waals contact within the metallocavitand. Geometry optimizations performed on the HO-Zn(μ_3-OH) complex and the $Zn_4(\mu_4\text{-O})$ complex + H_2O

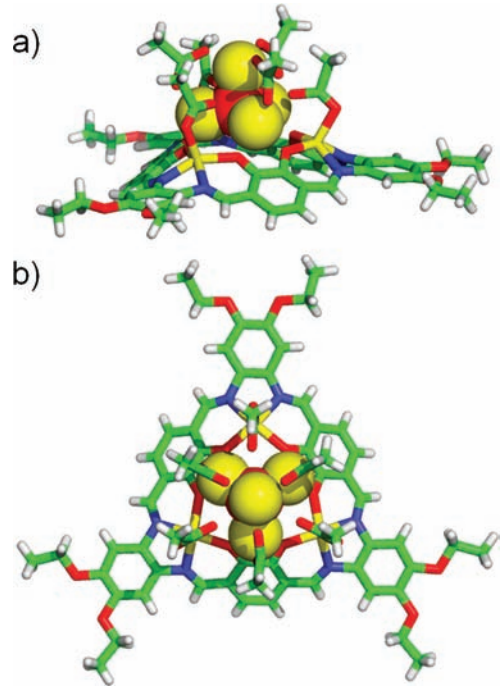

Figure 2. Solid-state molecular structure of **2a**. (a) Side-on view. (b) Top-down view. The central $Zn_4(\mu_4\text{-O})$ cluster is modeled as space filling. (C = green, N = blue, O = red, H = white, Zn = yellow).

Scheme 2. Equilibrium between the $Zn_4(\mu_4\text{-O})$ Complex + H_2O and the HO-Zn(μ_3-OH) Complex Investigated with DFT Computations[a]

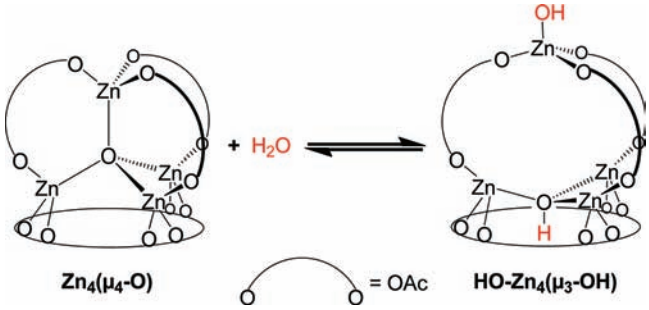

[a]Calculations indicate that the left side of the equilibrium is 100 kJ mol^{-1} more stable than the right side. The ring at the bottom of the cluster represents the trizinc macrocycle. Some acetate groups are omitted for clarity.

at the SDD/B98/D95(d,p) level of theory revealed that the $Zn_4(\mu_4\text{-O})$ complex + H_2O is 100 kJ mol^{-1} more stable than the HO-Zn(μ_3-OH) complex. These calculations are in good agreement with the experimental results that only provide evidence for the $Zn_4(\mu_4\text{-O})$ complex configuration. The optimized structure of the less stable HO-Zn(μ_3-OH) complex exhibits significant distortion from tetrahedral geometry of the capping zinc ion. Two of the upper acetate ligands exhibit longer Zn–O distances (2.019 and 2.029 Å) compared to the third Zn–O distance (1.989 Å) and the capping Zn–OH distance is 1.851 Å.

After confirming the solution geometry of heptazinc metallocavitands with computations, time-dependent DFT calculations were performed to fully interpret their electronic absorption spectra. Metallocavitands **2a–c** exhibit nearly identical absorption spectra in dichloromethane, showing two

dx.doi.org/10.1021/ic202049t | Inorg. Chem. 2012, 51, 3443–3453

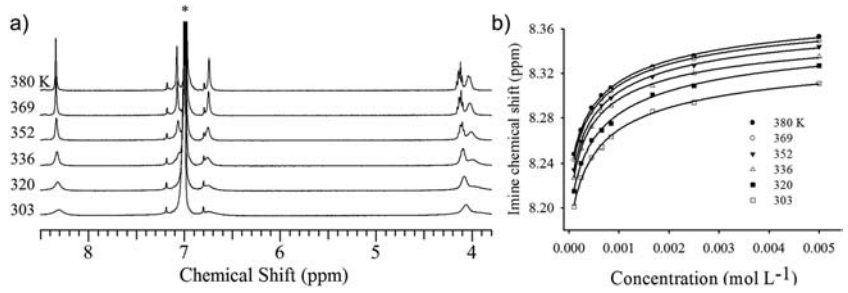

Figure 3. (a) VT ^{1}H NMR spectra of **2c** in *p*-xylene-d_{10} (5.0 mmol L^{-1}, 400 MHz, * denotes solvent). (b) Results of VTVC experiments of **2c** in *p*-xylene-d_{10} with nonlinear regressions used to calculated dimerization constants.

Table 1. Thermodynamic Parameters of Dimerization in Aromatic Solvents Calculated from VTVC ^{1}H NMR Spectroscopy

complex	solvent	K_{dim} 25 °C (mol L^{-1})[a]	$\Delta H°_{dim}$ (kJ mol^{-1})	$\Delta S°_{dim}$ (J mol^{-1} K^{-1})
2b (R = C_6H_{13})	toluene-d_8	110 ± 10	19 ± 2	103 ± 8
2c (R = C_8H_{17})	CD_2Cl_2	<1		
	C_6D_6	9 ± 3	24 ± 12	100 ± 34
	toluene-d_8	110 ± 10	10 ± 2	72 ± 5
	p-xylene-d_{10}	1200 ± 200	1 ± 3	60 ± 9

[a]Calculated at 25 °C from van't Hoff plots.

broad absorptions with λ_{max} = 414 and 347 nm and extinction coefficients in the 10^5 and 10^4 L mol^{-1} cm^{-1} range, respectively. Each spectrum strongly resembles the absorption spectrum of the metal-free parent macrocycle that has been previously calculated.[54]

The broadness of the λ_{max} absorptions and existence of small shoulders hinted that the spectra are a result of more than two simple transitions. Twelve Gaussian functions were needed to accurately reproduce the spectra (see Supporting Information, Figure 10). Transitions with large HOMO → LUMO contributions are very weak whereas the most intense low energy transitions involve HOMO-4 → LUMO and HOMO-3 → LUMO+1 excitations. The second most intense absorption is the result of many monoelectronic excitations with the largest contribution coming from the HOMO-6 → LUMO. Electron density in the frontier molecular orbitals is principally located on the catecholate aromatic rings of the macrocycle (see Supporting Information, Figure 11 for orbital diagrams). From HOMO-6 to LUMO+5 there is no electron density found on the zinc cluster making the entire absorption spectrum, from visible to near UV, because of the macrocyclic electronic structure.

Solution Dimerization. Metallocavitands **2b** and **2c** with hexyloxy and octyloxy substituents, respectively, are soluble in nonpolar organic solvents that enable ^{1}H NMR spectroscopic investigation of dimerization. For **2c**, a single imine resonance at 8.31 ppm, two aromatic resonances at 6.96 and 6.69 ppm, and one OCH_2 methylene resonance at 4.06 ppm are observed downfield of 4 ppm in the ^{1}H NMR spectrum in $CDCl_3$ indicating **2c** has 3-fold rotational symmetry in solution. Similar chemical shift values and 3-fold rotational symmetry were observed for **2b** in $CDCl_3$. The OCH_2 methylene protons of **2b** and **2c** are diastereotopic, and a complex ABX_2 coupling pattern is observed confirming the absence of a horizontal mirror plane. Although no solid-state structure has been acquired for **2b** or **2c**, ^{13}C NMR spectroscopy, MALDI-TOF-MS, FT-IR spectroscopy, electronic absorption, and elemental analysis all support the assertion that they share the same metallocavitand structure observed for **2a** in the solid state.

In $CDCl_3$ and CD_2Cl_2 the proton resonances of **2c** are sharp; in C_6D_6, toluene-d_8, and *p*-xylene-d_{10}, however, the aromatic and imine resonances are significantly broadened. This resonance broadening, indicative of a dynamic process occurring on the NMR time scale, encouraged us to further investigate the self-association of **2c**.

Figure 3a depicts a series of ^{1}H NMR spectra of **2c** at various temperatures in *p*-xylene-d_{10}. As the temperature of a solution of **2c** in *p*-xylene-d_{10} is increased, the aromatic and imine resonances narrow and shift downfield while the resolution of the diastereotopic methylene protons adjacent to oxygen on the periphery improves. Interestingly, there is a significant difference in the effects of temperature on the two diastereotopic protons; although both appear sharper at elevated temperature, *J*-coupling is only resolved for the downfield resonance.

In an effort to slow the exchange rate of **2c** below the coalescence temperature and reach an intermediate exchange regime, a ^{1}H NMR spectrum of **2c** was collected at −70 °C in toluene-d_8; even at this temperature, however, the resonances remain coalesced. Rapid exchange, solvent freezing point, and limited metallocavitand solubility prevented measurement of the coalescence temperature of **2c** in C_6D_6, toluene-d_8, and *p*-xylene-d_{10}. To investigate the thermodynamic parameters of dimerization in a fast exchange regime, variable-temperature variable-concentration (VTVC) ^{1}H NMR spectroscopic experiments were conducted in CD_2Cl_2, C_6D_6, toluene-d_8, and *p*-xylene-d_{10}.

A dimerization model fit well to the measured change in imine chemical shift over a range of VTVC ^{1}H NMR spectra (Figure 3b).[38] The quality of fit enabled extraction of dimerization constants at a variety of temperatures. Thermodynamic parameters for self-association were determined from van't Hoff plots. The experimental dimerization constants, enthalpies, and entropies of dimerization for compounds **2c** and **2b** are shown in Table 1.

Interesting trends are observed for the thermodynamic data. First, there is no dimerization observed in CD_2Cl_2 (or in $CDCl_3$). Aromatic solvents, however, facilitate dimerization to varying degrees. The extent of dimerization is low in benzene,

dx.doi.org/10.1021/ic202049t | Inorg. Chem. 2012, 51, 3443−3453

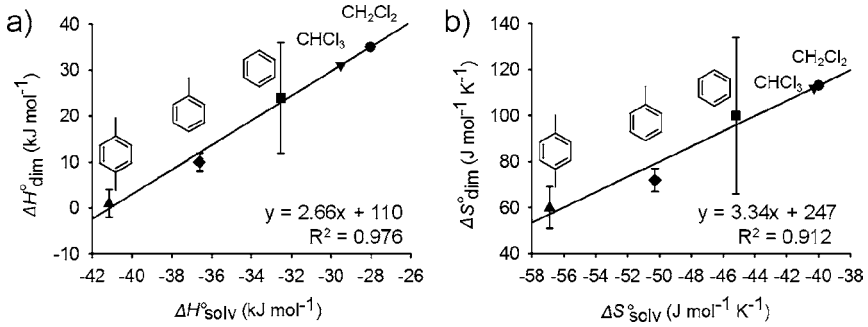

Figure 4. Experimentally determined thermodynamic parameters, (a) $\Delta H°_{dim}$ and (b) $\Delta S°_{dim}$,[61] for dimerization of **2c** compared with the thermodynamic parameters for autosolvation of one mole of solvent in the same solvent (benzene, toluene, and *p*-xylene). The linear correlations were calculated using only the benzene, toluene, and *p*-xylene data and are plotted with the calculated equations and R^2 values. $CHCl_3$ and CH_2Cl_2 data points were added to the trend lines using the autosolvation thermodynamic parameters, not experimental data.

but increases by an order of magnitude with each additional methyl substituent (toluene and *p*-xylene). Second, dimerization in both toluene and *p*-xylene shows decreases in enthalpy and entropy from benzene of approximately 10 kJ mol^{-1} and 20 J K^{-1} mol^{-1} per methyl group, respectively. Surprisingly, dimerization of these metallocavitands is an entropy-driven process in aromatic solvents. Most self-association processes are enthalpy-driven and entropy-opposed since the dimers are often held together by strong intermolecular interactions (e.g., hydrogen bonds) and order is generally being imparted on the system.

Entropy-driven dimerization is uncommon but has been observed for other cavitand systems such as Cram's velcrands,[55] Rebek's molecular capsules,[56] and heptacadmium metallocavitands.[23] In these instances the entropy-driven process is explained by expulsion of solvent molecules from monomers upon dimerization, similar to the hydrophobic effect.[57] For metallocavitands **2b–c**, it is possible that in aromatic solvents, the solvent forms π–π interactions with the bowl of the metallocavitand, and this solvent is expelled from the bowl upon dimerization, increasing the net entropy in the system.

Although the experimentally determined thermodynamic parameters strongly suggest that expulsion of solvent from the monomer's bowl-like cavity promotes dimerization, VTVC ^{1}H NMR spectroscopic experiments were conducted on **2b** in toluene-d_8 to gauge the impact of peripheral chain length on self-association. Entropy-driven, enthalpy-opposed dimerization is also observed for **2c** in toluene-d_8 (Table 1).

Analysis of the Thermodynamics of Dimerization in Solution. Although entropy-driven dimerization has been previously attributed to the loss of solvent from the interior of a cavitand, to the best of our knowledge, no quantitative analysis has been performed to untangle the individual roles of solvent-monomer, solvent–solvent, and monomer–monomer interactions in entropy-driven dimerization. The dimerization thermodynamics of **2c** clearly exhibit a trend (Table 1) in aromatic solvents that, when analyzed appropriately, provides some initial quantitative insights into the entropy-driven dimerization process. We provide a detailed derivation here to clarify our analysis for the reader.

To extract meaningful information from the trends in $\Delta H°_{dim}$ and $\Delta S°_{dim}$ observed for **2c**, we first considered the "autosolvation" of the solvent molecules that are associated with the monomer **2c**, where autosolvation is defined as the dissolution of a single solvent molecule into the identical bulk solvent.[58] The dimerization reaction in solution is

$$(B\underline{S}_n)_{sol} + (B\underline{S}_n)_{sol} \rightleftharpoons (B\underline{S}_mB)_{sol} + (2n - m)\underline{S}_{sol}$$

where B is the bowl (monomeric metallocavitand), $\underline{S}$ is a solvent molecule (where there are n solvent molecules interacting with the monomer, and m solvent molecules encapsulated in the dimer; we use underlined $\underline{S}$ to represent solvent, thus distinguishing it from S for entropy). In the dimerization process, $(2n - m)$ $\underline{S}$ molecules move from the solvated bowl $(B\underline{S}_n)_{sol}$ into the solvent. Similar to the Born–Haber cycle, Hess's law may be applied to the dimerization process giving the equilibria depicted below:

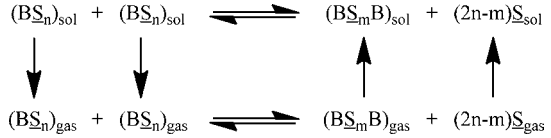

Implementing the equilibria from the solution phase to the gas phase and back into the solution phase enables the contribution from the solvation of a solvent molecule in the same solvent $(2n - m)\underline{S}_{gas} \rightarrow (2n - m)\underline{S}_{sol}$ (autosolvation) to be used in the later derivations. These autosolvation values of one mole of solvent molecule in the same solvent have been determined for CH_2Cl_2, $CHCl_3$, benzene, toluene and *p*-xylene.[59,60] Interestingly, plotting the experimentally determined thermodynamic parameters ($\Delta H°$, $\Delta S°$) of dimerization in benzene, toluene, and *p*-xylene (Table 1) versus the autosolvation thermodynamics of the solvents shows the linear relationship depicted in Figure 4, suggesting autosolvation may play a significant role in the dimerization process. Linear trend lines were calculated using only the experimental and autosolvation data for benzene, toluene and *p*-xylene.

Assuming the linear correlation observed for aromatic solvents is applicable to other solvents, it is possible to "evaluate" the enthalpy and entropy of dimerization in CH_2Cl_2 and $CHCl_3$ starting from the autosolvation thermodynamic parameters. From the linear regressions, K_{dim} in CH_2Cl_2 and $CHCl_3$ are 1 and 3 mol L^{-1}, respectively. These dimerization constants are so low that at equilibrium the concentration of dimer would be undetectable by NMR spectroscopy, as we observed experimentally. A summary of the dimerization thermodynamics calculated from the linear regressions in Figure 4 may be found in Table 2. The calculated values correspond surprisingly well with the experimentally determined dimerization constants.

dx.doi.org/10.1021/ic202049t | *Inorg. Chem.* 2012, 51, 3443–3453

Table 2. Calculated K_{dim}, ΔH°_{dim}, ΔS°_{dim}, and ΔG°_{dim} in Different Solvents Using the Linear Regression Lines from Figure 4

solvent	K_{dim} (mol L^{-1})[a]	ΔH°_{dim} (kJ mol^{-1})	ΔS°_{dim} (J mol^{-1} K^{-1})	ΔG°_{dim} (kJ mol^{-1})
CH_2Cl_2	1	35	113	1
$CHCl_3$	3	31	112	−3
benzene	10	23	96	−6
toluene	103	12	79	−11
p-xylene	936	0	57	−17

[a]At 25 °C.

The linear fit in Figure 4 suggests that the thermodynamic parameters can be described as equations for a line:

$$\Delta H_{sol}^{dim} = k_H \cdot \Delta H_{\underline{S}}^{solv} + a_H \quad (1)$$

$$\Delta S_{sol}^{dim} = k_S \cdot \Delta S_{\underline{S}}^{solv} + a_S \quad (2)$$

Experimentally measured ΔH°_{dim} and ΔS°_{dim} are equivalent to ΔH_{sol}^{dim} and ΔS_{sol}^{dim}, respectively.[62] In eqs 1 and 2, $\Delta H_{\underline{S}}^{solv}$ and $\Delta S_{\underline{S}}^{solv}$ come from the autosolvation of solvent molecules that are released by the complex $B\underline{S}_nB$ and re-enter into the bulk of the solvent upon dimerization.[62] To impart meaning to the linear regression parameters k_H, a_H, k_S, and a_S (slopes and intercepts of enthalpy and entropy plots from the regression lines in Figure 4, respectively) we begin the following derivation from the Born−Haber cycle:

$$\Delta G_{sol}^{dim} = \Delta G_{gas}^{dim} + (\Delta G_{B\underline{S}_mB}^{solv} - 2\Delta G_{B\underline{S}_n}^{solv}) + (2n - m)\Delta G_{\underline{S}}^{solv}$$

This may be separated as

$$\Delta H_{sol}^{dim} = \Delta H_{gas}^{dim} + (\Delta H_{B\underline{S}_mB}^{solv} - 2\Delta H_{B\underline{S}_n}^{solv}) + (2n - m)\Delta H_{\underline{S}}^{solv} + \Delta H^{(gas\rightarrow solv)}_{(relax)}$$

and

$$\Delta S_{sol}^{dim} = \Delta S_{gas}^{dim} + (\Delta S_{B\underline{S}_mB}^{solv} - 2\Delta S_{B\underline{S}_n}^{solv}) + (2n - m)\Delta S_{\underline{S}}^{solv}$$

As far as the solvation is concerned, the ΔH contribution to $\Delta G_{B\underline{S}mB}^{solv}$ and $\Delta G_{B\underline{S}n}^{solv}$ does not depend strongly on the particular solvent, $\underline{S}$. The capsule and monomeric bowl are far larger than the aromatic solvent molecules, both from the point of view of their volume and number of electrons. Therefore, the difference in perturbation induced by the solute (monomeric bowl or capsule) to the solvent "structure" of different solvents should be very small. The perturbation is given by the interactions between each $B\underline{S}_mB$ and $B\underline{S}_n$ separately with solvent, and this should depend on the exposed surface of B, i.e., the "external" part of the monomer $B\underline{S}_n$ and the capsule $B\underline{S}_mB$. A further contribution is due to the enthalpy to dig a "hole" in the solvent.[63] In the case of $B\underline{S}_mB$, this contribution can be assumed to be twice the value of $B\underline{S}_n$.[64,65] Hence,

$$(\Delta H_{B\underline{S}_mB}^{solv} - 2\Delta H_{B\underline{S}_n}^{solv}) \approx 0$$

and

$$\Delta H^{(gas\rightarrow solv)}_{(relax)} = (\Delta H_{B\underline{S}_mB}^{relax} - 2\Delta H_{B\underline{S}_n}^{relax}) \approx \Delta H^{(gas\rightarrow solv)}_{(relax)}{}^{dim}$$

This last contribution, $\Delta H^{(gas\rightarrow solv)}_{(relax)}$, is due to the geometrical reorganization of the molecules from the gas phase to the equilibrium geometry in solution. This contribution is mainly due to the dimer because it is not as rigid as the monomer.[66]

The entropy change, $\Delta S_{B\underline{S}mB}^{solv} - 2\,\Delta S_{B\underline{S}n}^{solv}$, is related to the different behavior of solvent molecules around the solutes $B\underline{S}_mB$ and $B\underline{S}_n$. We can assume that the contribution to the solvation entropy coming from the external part of the capsule $B\underline{S}_mB$ is almost twice that around the bowl, $B\underline{S}_n$, with the solvent molecules inside.

$$(\Delta S_{B\underline{S}_mB}^{solv} - 2\Delta S_{B\underline{S}_n}^{solv}) \approx 0$$

Hence, the enthalpy and entropy of the solvation process can be cast in the form

$$\Delta H_{sol}^{dim} = (\Delta H_{gas}^{dim} + \Delta H^{(gas\rightarrow solv)}_{(relax)}{}^{dim}) + (2n - m)\Delta H_{\underline{S}}^{solv} \quad (3)$$

$$\Delta S_{sol}^{dim} = \Delta S_{gas}^{dim} + (2n - m)\Delta S_{\underline{S}}^{solv} \quad (4)$$

Therefore, $(\Delta G_{B\underline{S}mB}^{solv} - 2\,\Delta G_{B\underline{S}n}^{solv}) \approx 0$ and $\Delta G_{sol}^{dim} = \Delta G_{gas}^{dim} + (2n - m)\,\Delta G_{\underline{S}}^{solv}$.

By comparing eq 1 with eq 3 and eq 2 with eq 4, a physical meaning may be established for the regression line parameters k_H, a_H, k_S, and a_S, obtained from the linear regressions in Figure 4. The k_H and k_S values, the slopes of the graphs in Figure 4, are similar, 2.66 and 3.34, respectively, and represent the number of solvent molecules being released into solution upon dimerization $(2n - m)$. This means that from the plots of ΔH° and ΔS° we get similar results for the k_H and k_S values even though they are obtained from different data compilations. SCXRD data suggest that inside each capsule, $B\underline{S}_mB$, there is only enough space for one solvent molecule ($m = 1$). If this behavior is preserved in solution, the number of solvent molecules (n) inside the monomeric metallocavitand in solution, $B\underline{S}_n$, is about 2 (1.8 from k_H and 2.2 from k_S).[67]

Furthermore, according to the comparison of eqs 1 with 3 and 2 with 4 and by extrapolating to $\Delta H_{\underline{S}}^{solv}$ or $\Delta S_{\underline{S}}^{solv} = 0$ (i.e., the intercepts of the lines in Figure 4), we find that $\Delta H_{gas}^{dim} + \Delta H^{(gas\rightarrow solv)}_{(relax)}{}^{dim}$ and ΔS_{gas}^{dim} are +110 kJ mol^{-1} and +247 J mol^{-1} K^{-1}, respectively. These values suggest that (1) the dimerization process might also be enthalpy-opposed and entropy-driven in the gas phase; and (2) the trend of the thermodynamic parameters in solution is due to the thermodynamics of the autosolvation process of the solvent molecules.

From the preceding derivations, it is also possible to speculate about the gas phase enthalpy of dimerization (ΔH_{gas}^{dim}) and about the interaction between the two monomeric bowls, solvent molecules that are hosted in the bowls, and capsule without the contribution of the bulk solvent. Looking at the relationship $\Delta H_{gas}^{dim} + \Delta H^{(gas\rightarrow solv)}_{(relax)}{}^{dim}$, it is possible that the two bowls may be attracted to each other in

dx.doi.org/10.1021/ic202049t | Inorg. Chem. 2012, 51, 3443−3453

the gas phase (enthalpy favored); however, when they prepare for dissolution, reaching their final relative position (probably closer together than in gas phase) they are destabilized by the reorganization enthalpy $\Delta H^{(\text{gas}\rightarrow\text{solv})}{}_{(\text{relax})}{}^{\text{dim}}$. Dimerization in the gas phase follows the equation:

$$(\text{B}\underline{\text{S}}_n)_{\text{gas}} + (\text{B}\underline{\text{S}}_n)_{\text{gas}} \rightleftharpoons (\text{B}\underline{\text{S}}_m\text{B})_{\text{gas}} + (2n - m)\underline{\text{S}}_{\text{gas}}$$

Let the interaction enthalpy of one solvent molecule $\underline{\text{S}}$ inside the bowl be defined as $K_{\text{B}\underline{\text{S}}}{}^{\text{gas}}$, and assume that (1) solvent interacts equally with the both halves of the capsule[68] in the dimer so its interaction enthalpy should be close to 2 $K_{\text{B}\underline{\text{S}}}{}^{\text{gas}}$ (i.e., twice the value of the interaction enthalpy of solvent inside the monomeric bowl); and (2) the interaction enthalpy between each solvent molecule with the bowl is almost the same in case of benzene, toluene and *p*-xylene.[69] Hence we have

$$\Delta H_{\text{B}\underline{\text{S}}_m\text{B}}{}^{\text{gas}} - 2\Delta H_{\text{B}\underline{\text{S}}_n}{}^{\text{gas}} \approx 2mK_{\text{B}\underline{\text{S}}}{}^{\text{gas}} - 2nK_{\text{B}\underline{\text{S}}}{}^{\text{gas}} \quad (5)$$

Furthermore, assuming that the interaction enthalpy between the two bowls ($K_{\text{BB}}{}^{\text{gas}}$) in the capsule is a slowly varying function of $\underline{\text{S}}$ ($\underline{\text{S}}$ might influence the distance between the two B), or almost independent of $\underline{\text{S}}$, then $\Delta H_{\text{B}\underline{\text{S}}_m\text{B}}{}^{\text{gas}} - 2\ \Delta H_{\text{B}\underline{\text{S}}_n}{}^{\text{gas}}$ is close to $2(m - n)K_{\text{B}\underline{\text{S}}}{}^{\text{gas}}$ plus the contribution $K_{\text{BB}}{}^{\text{gas}}$ coming from the B−B interaction in the gas phase at the equilibrium geometry in solution.[70] Therefore,

$$\Delta H_{\text{gas}}{}^{\text{dim}} + \Delta H^{(\text{gas}\rightarrow\text{solv})}{}_{(\text{relax})}{}^{\text{dim}} = K_{\text{BB}}{}^{\text{gas}} + 2(m - n)K_{\text{B}\underline{\text{S}}}{}^{\text{gas}} \quad (6)$$

Assuming from the earlier derivation that $m = 1$ and $n = 2$, this becomes

$$\Delta H_{\text{gas}}{}^{\text{dim}} + \Delta H^{(\text{gas}\rightarrow\text{solv})}{}_{(\text{relax})}{}^{\text{dim}} = (K_{\text{BB}}{}^{\text{gas}}) - 2K_{\text{B}\underline{\text{S}}}{}^{\text{gas}}$$

If $K_{\text{B}\underline{\text{S}}}{}^{\text{gas}}$ is assumed equal to the computed DFT interaction enthalpy of a benzene molecule inside the bowl at SDD/D95(d)/M06 level of theory which amounts to −32.7 kJ mol^{-1} (taking into account the BSSE), then

$$K_{\text{BB}}{}^{\text{gas}} = \Delta H_{\text{gas}}{}^{\text{dim}} + \Delta H^{(\text{gas}\rightarrow\text{solv})}{}_{(\text{relax})}{}^{\text{dim}} + 2K_{\text{B}\underline{\text{S}}}{}^{\text{gas}} \quad \text{is} \quad \approx 45\ \text{kJ mol}^{-1}$$

These results further suggest that even in the gas phase the interaction between the two bowls might be also enthalpy-opposed.

Metallocavitand-C_{60} Host−Guest Complexation. Owing to their favorable electron accepting ability, fullerenes have become increasingly important molecules in the fabrication of efficient organic electronic and photovoltaic devices.[71] Strong interactions between fullerenes and concave or pincer-shaped host molecules with binding constants as large as 10^8 L mol^{-1} have been reported.[72] These supramolecular interactions have enabled selective separation of a single fullerene from mixtures,[73] preparation of supramolecular electroactive polymers,[74] and preparation of noncovalent photoactive donor−acceptor dyads.[75] Electron donating host molecules generally bind fullerenes in an enthalpy-favored, entropy-opposed manner, and little is known about entropy-driven fullerene complexation.

Metallocavitand **2c** is concave, and molecular modeling suggests that up to three metallocavitands may bind with a single C_{60} molecule (See Supporting Information, Figure 15). Qualitative analysis of C_{60} binding was performed by ^{1}H NMR spectroscopy in $CDCl_3$, C_6D_6, and toluene-d_8. In both C_6D_6 and toluene-d_8 the imine, aromatic, and methylene resonances shifted upon addition of C_{60}, evidence for host−guest complexation as illustrated in Figure 5. Interestingly, much

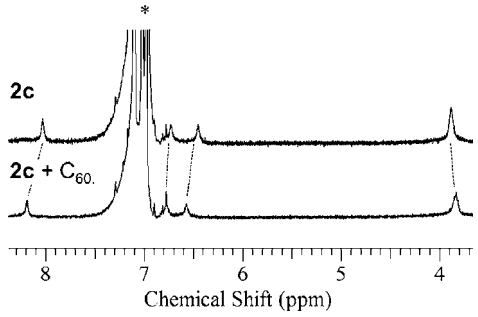

Figure 5. ^{1}H NMR spectra of **2c** in toluene-d_8 before (top) and after (bottom) addition of 5 equiv of C_{60}. The concentration of **2c** is 0.50 mmol L^{-1} in both spectra (400 MHz, * denotes solvent).

like dimerization, in $CDCl_3$ no change was observed in the ^{1}H NMR spectrum of **2c** upon addition of C_{60}, suggesting the metallocavitand-C_{60} interaction may be entropy controlled.

Quantification of the **2c**·C_{60} interaction was significantly hindered by the presence of competing equilibria. VC ^{1}H NMR spectroscopic experiments in toluene-d_8 fit reasonably well to a 1:1 binding model and gave association constants of about 10^3 L mol^{-1}. However, a 1:1 **2c**:C_{60} binding model is likely an oversimplification of the system. A Job plot constructed from titration experiments in toluene-d_8 showed a broad maximum from 1:1 to 3:1 for **2c**:C_{60} (Supporting Information, Figure 9). We hypothesize that five different species, **2c** monomer, **2c** dimer, **2c**·C_{60}, (**2c**)$_2$·C_{60}, and (**2c**)$_3$·C_{60}, are all present in solution as shown in Scheme 3. The fast exchange regime observed for complexes of **2c** and C_{60} limited measurements by both NMR and UV−vis spectroscopy to a single variable, preventing further analysis. Although quantitative information about the **2c**·C_{60} interaction was elusive, our qualitative results

Scheme 3. Hypothesized Competing Equilibria in a Solution of 2c and C_{60}

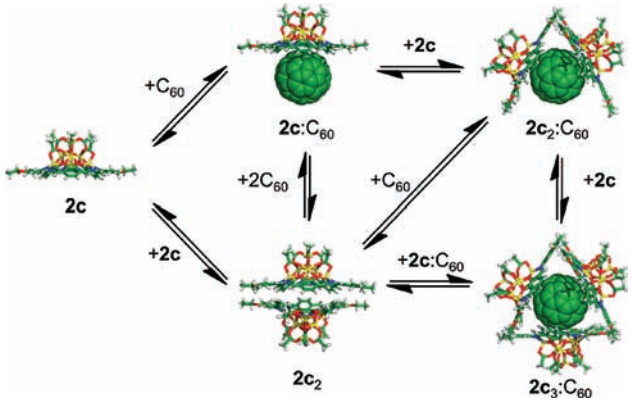

dx.doi.org/10.1021/ic202049t | Inorg. Chem. 2012, 51, 3443−3453

in different solvents suggest that entropy and autosolvation may be important factors in driving **2c**·C_{60} interactions.

CONCLUSIONS

Heptazinc metallocavitands templated by Schiff base macrocycles represent an emerging class of container molecules that exhibit interesting supramolecular behavior. Solid-state metallocavitand capsules were observed by SCXRD and show potential for host−guest metal−ligand interactions. These bowl-shaped molecules dimerize in a face-to-face manner in aromatic solvents (benzene, toluene, *p*-xylenes). Variable-temperature, variable-concentration NMR experiments showed that the dimerization of the molecules is an entropy-driven, enthalpy-opposed event. Trends in the equilibrium constants for dimerization in solution were explained by comparison to the thermodynamics of autosolvation of the guest molecules. That is, the thermodynamics of dimerization are dominated (both $\Delta H°$ and $\Delta S°$) by the autosolvation of molecules of solvent that are inside the bowls and released during dimerization. From this analysis, we estimated that two solvent molecules are associated inside the monomeric metallocavitand and dimerization of heptazinc metallocavitands is also entropy-driven and enthalpy-opposed in the gas phase. Moreover, the autosolvation explained why dimerization is not observed for the metallocavitands in CH_2Cl_2 or $CHCl_3$.

DFT calculations confirmed that the $Zn_4(\mu_4\text{-O})$ cluster geometry observed in the solid state is energetically preferred in solution over a similar HO-$Zn_4(\mu_3\text{-OH})$ cluster analogous to that previously observed in heptacadmium metallocavitands. Metallocavitand **2c** also forms host−guest complexes with C_{60}, and the solvent dependence of **2c**·C_{60} complex formation suggests that entropy and autosolvation may be the driving forces for some C_{60} host−guest interactions. Expanding the host−guest chemistry of heptazinc metallocavitands to enable host−guest catalysis at the exposed Zn sites within the cavity is of interest to us.

ASSOCIATED CONTENT

Supporting Information

VTVC ^{1}H NMR data, Job plot, results of DFT calculations, molecular models, and X-ray crystallographic data (CIF) for **2a**. This material is available free of charge via the Internet at http://pubs.acs.org.

AUTHOR INFORMATION

Corresponding Author

*E-mail: mmaclach@chem.ubc.ca (M.J.M.), francesco.lelj@unibas.it (F.L.).

Notes

The authors declare no competing financial interest.

ACKNOWLEDGMENTS

We are grateful to NSERC (Discovery Grant) for funding. P.D.F. thanks UBC for a Pacific Century Graduate Fellowship. F.L. is grateful to INSTM and the Project "Call for Ideas" of Università della Basilicata for 2010 for financial support and the Department of Chemistry of University of British Columbia for the warm hospitality.

REFERENCES

(1) Cram, D. J. *Science* **1983**, *219*, 1177−1183.

(2) (a) Melegari, M.; Suman, M.; Pirondini, L.; Moiani, D.; Massera, C.; Ugozzoli, F.; Kalenius, E.; Vainiotalo, P.; Mulatier, J.-C.; Dutasta, J.-P.; Dalcanale, E. *Chem.—Eur. J.* **2008**, *14*, 5772−5779. (b) Ballester, P.; Sarmentero, M. A. *Org. Lett.* **2006**, *8*, 3477−3480. (c) Kim, S. K.; Moon, B.-S.; Park, J. H.; Seo, Y. I.; Koh, H. S.; Yoon, Y. J.; Lee, K. D.; Yoon, J. *Tetrahedron Lett.* **2005**, *46*, 6617−6620. (d) Pinalli, R.; Suman, M.; Dalcanale, E. *Eur. J. Org. Chem.* **2004**, 451−462.

(3) (a) Taratula, O.; Dmochowski, I. J. *Curr. Opin. Chem. Biol.* **2010**, *14*, 97−104. (b) Chambers, J. M.; Hill, P. A.; Aaron, J. A.; Han, Z.; Christianson, D. W.; Kuzma, N. N.; Dmochowski, I. J. *J. Am. Chem. Soc.* **2009**, *131*, 563−569. (c) Schlundt, A.; Kilian, W.; Beyermann, M.; Sticht, J.; Guenther, S.; Hoepner, S.; Falk, K.; Roetzschke, O.; Mitschang, L.; Freund, C. *Angew. Chem., Int. Ed.* **2009**, *48*, 4142−4145.

(4) (a) Hooley, R. J.; Restorp, P.; Iwasawa, T.; Rebek, J. Jr. *J. Am. Chem. Soc.* **2007**, *129*, 15639−15643. (b) Hooley, R. J.; Iwasawa, T.; Rebek, J. Jr. *J. Am. Chem. Soc.* **2007**, *129*, 15330−15339.

(5) (a) Gibb, C. L. D.; Sundaresan, A. K.; Ramamurthy, V.; Gibb, B. C. *J. Am. Chem. Soc.* **2008**, *130*, 4069−4080. (b) Kaanumalle, L. S.; Gibb, C. L. D.; Gibb, B. C.; Ramamurthy, V. *Org. Biomol. Chem.* **2007**, *5*, 236−238. (c) Natarajan, A.; Kaanumalle, L. S.; Jockusch, S.; Gibb, C. L. D.; Gibb, B. C.; Turro, N. J.; Ramamurthy, V. *J. Am. Chem. Soc.* **2007**, *129*, 4132−4133. (d) Kaanumalle, L. S.; Gibb, C. L. D.; Gibb, B. C.; Ramamurthy, V. *J. Am. Chem. Soc.* **2005**, *127*, 3674−3675. (e) Kaanumalle, L. S.; Gibb, C. L. D.; Gibb, B. C.; Ramamurthy, V. *J. Am. Chem. Soc.* **2004**, *126*, 14366−14367.

(6) (a) Hooley, R. J.; Rebek, J. Jr. *Chem. Biol.* **2009**, *16*, 255−264. (b) Pinacho Crisostomo, F. R.; Lledo, A.; Shenoy, S. R.; Iwasawa, T.; Rebek, J. Jr. *J. Am. Chem. Soc.* **2009**, *131*, 7402−7410. (c) Kamioka, S.; Ajami, D.; Rebek, J. Jr. *Chem. Commun.* **2009**, 7324−7326. (d) Shenoy, S. R.; Pinacho Crisóstomo, F. R.; Iwasawa, T.; Rebek, J. Jr. *J. Am. Chem. Soc.* **2008**, *130*, 5658−5659.

(7) (a) Oshovsky, G. V.; Reinhoudt, D. N.; Verboom, W. *J. Am. Chem. Soc.* **2006**, *128*, 5270−5278. (b) Corbellini, F.; van Leeuwen, F. W. B.; Beijleveld, H.; Kooijman, H.; Spek, A. L.; Verboom, W.; Crego-Calama, M.; Reinhoudt, D. N. *New J. Chem.* **2005**, *29*, 243−248. (c) Vysotsky, M. O.; Mogck, O.; Rudzevich, Y.; Shivanyuk, A.; Böhmer, V.; Brody, M. S.; Cho, Y. L.; Rudkevich, D. M.; Rebek, J. Jr. *J. Org. Chem.* **2004**, *69*, 6115−6120. (d) Gibb, C. L. D.; Gibb, B. C. *J. Am. Chem. Soc.* **2004**, *126*, 11408−11409. (e) Cram, D. J.; Choi, H.-J.; Bryant, J. A.; Knobler, C. B. *J. Am. Chem. Soc.* **1992**, *114*, 7748−7765.

(8) (a) Cave, G. W. V.; Antesberger, J.; Barbour, L. J.; McKinlay, R. M.; Atwood, J. L. *Angew. Chem., Int. Ed.* **2004**, *43*, 5263−5266. (b) MacGillivray, L. R.; Atwood, J. L. *Nature* **1997**, *389*, 469−472.

(9) (a) Yebeutchou, R. M.; Tancini, F.; Demitri, N.; Geremia, S.; Mendichi, R.; Dalcanale, E. *Angew. Chem., Int. Ed.* **2008**, *47*, 4504−4508. (b) Castellano, R. K.; Rudkevich, D. M.; Rebek, J. Jr. *Proc. Natl. Acad. Sci. U.S.A.* **1997**, *94*, 7132−7137.

(10) Reviews on cavitand coordination complexes: (a) Dalgarno, S. J.; Power, N. P.; Atwood, J. L. *Coord. Chem. Rev.* **2008**, *252*, 825−841. (b) Lenthall, J. T.; Steed, J. W. *Coord. Chem. Rev.* **2007**, *251*, 1747−1760. (c) Hapiot, F.; Tilloy, S.; Monflier, E. *Chem. Rev.* **2006**, *106*, 767−781. (d) Jeunesse, C.; Armspach, D.; Matt, D. *Chem. Commun.* **2005**, 5603−5614. (e) Atwood, J. L.; Holman, K. T.; Steed, J. W. *Chem. Commun.* **1996**, 1401−1407.

(11) Recent literature: (a) Zaborova, E.; Deschamp, J.; Guieu, S.; Blériot, Y.; Poli, G.; Ménand, M.; Madec, D.; Prestat, G.; Sollogoub, M. *Chem. Commun.* **2011**, *47*, 9206−9208. (b) Guieu, S.; Zaborova, E.; Blériot, Y.; Poli, G.; Jutand, A.; Madec, D.; Prestat, G.; Sollogoub, M. *Angew. Chem., Int. Ed.* **2010**, *49*, 2314−2318. (c) Huerta, E.; Metselaar, G. A.; Fragoso, A.; Santos, E.; Bo, C.; de Mendoza, J. *Angew. Chem., Int. Ed.* **2007**, *46*, 202−205. (d) Fox, D. O.; Cookson, J.; Wilkinson, E. J. S.; Drew, M. G. B.; MacLean, E. J.; Teat, S. J.; Beer, P. D. *J. Am. Chem. Soc.* **2006**, *128*, 6990−7002. (e) Armspach, D.; Matt, D.; Peruch, F.; Lutz, P. *Eur. J. Inorg. Chem.* **2003**, 805−809. (f) Yang, J.; Gabriele, B.; Belvedere, S.; Huang, Y.; Breslow, R. *J. Org. Chem.* **2002**, *67*, 5057−5067. (g) Fox, O. D.; Drew, M. G. B.; Wilkinson, E. J. S.; Beer, P. D. *Chem. Commun.* **2000**, 391−392.

(12) Monnereau, L.; Sémeril, D.; Matt, D. *Chem. Commun.* **2011**, *47*, 6626−6628.

(13) Richeter, S.; Rebek, J. Jr. *J. Am. Chem. Soc.* **2004**, *126*, 16280–16281.
(14) Zelder, F. H.; Salvio, R.; Rebek, J. Jr. *Chem. Commun.* **2006**, 1280–1282.
(15) Zelder, F. H.; Rebek, J. Jr. *Chem. Commun.* **2006**, 753–754.
(16) (a) Gallant, A. J.; Hui, J.K.-H.; Zahariev, F. E.; Wang, Y. A.; MacLachlan, M. J. *J. Org. Chem.* **2005**, *70*, 7936–7946. (b) Gallant, A. J.; MacLachlan, M. J. *Angew. Chem., Int. Ed.* **2003**, *42*, 5307–5310. (c) Akine, S.; Taniguchi, T.; Nabeshima, T. *Tetrahedron Lett.* **2001**, *42*, 8861–8864.
(17) Frischmann, P. D.; MacLachlan, M. J. *Comments Inorg. Chem.* **2008**, *29*, 26–45.
(18) (a) Dolain, C.; Hatakeyama, Y.; Sawada, T.; Tashiro, S.; Fujita, M. *J. Am. Chem. Soc.* **2010**, *132*, 5564–5565. (b) Garon, C. N.; Gorelsky, S. I.; Sigouin, O.; Woo, T. K.; Fontaine, F.-G. *Inorg. Chem.* **2009**, *48*, 1699–1710. (c) Sigouin, O.; Garon, C. N.; Delaunais, G.; Yin, X.; Woo, T. K.; Decken, A.; Fontaine, F.-G. *Angew. Chem., Int. Ed.* **2007**, *46*, 4979–4982. (d) Tashiro, S.; Tominaga, M.; Yamaguchi, Y.; Kato, K.; Fujita, M. *Angew. Chem., Int. Ed.* **2006**, *45*, 241–244.
(19) (a) Rochat, S.; Grote, Z.; Severin, K. *Org. Biomol. Chem.* **2009**, *7*, 1147–1153. (b) Galindo, M. A.; Houlton, A.; Clegg, W.; Harrington, R. W.; Dobado, J.; Santoyo-Gonzalez, F.; Linares, F.; Romero, M. A.; Navarro, J. A. R. *Chem. Commun.* **2008**, 3735–3737.
(20) (a) Lindsay, V. N. G.; Lin, W.; Charette, A. B. *J. Am. Chem. Soc.* **2009**, *131*, 16383–16385. (b) DeAngelis, A.; Dmitrenko, O.; Yap, G. P. A; Fox, J. M. *J. Am. Chem. Soc.* **2009**, *131*, 7230–7231. (c) Jacques, B.; Dro, C.; Bellemin-Laponnaz, S.; Wadepohl, H.; Gade, L. H. *Angew. Chem., Int. Ed.* **2008**, *47*, 4546–4550. (d) Kaess, S.; Gregor, T.; Kersting, B. *Angew. Chem., Int. Ed.* **2006**, *45*, 101–104. (e) Steinfeld, G.; Lozan, V.; Kersting, B. *Angew. Chem., Int. Ed.* **2003**, *42*, 2261–2263.
(21) Yu, S.-Y.; Kusukawa, T.; Biradha, K.; Fujita, M. *J. Am. Chem. Soc.* **2000**, *122*, 2665–2666.
(22) Shibasaki, M., Yamamoto, Y., Eds.; *Multimetallic Catalysts in Organic Synthesis*; Wiley-VCH: Weinheim, Germany, 2004.
(23) (a) Frischmann, P. D.; Facey, G. A.; Ghi, P. Y.; Gallant, A. J.; Bryce, D. L.; Lelj, F.; MacLachlan, M. J. *J. Am. Chem. Soc.* **2010**, *132*, 3893–3908. (b) Frischmann, P. D.; MacLachlan, M. J. *Chem. Commun.* **2007**, 4480–4482.
(24) Vickers, S. M.; Frischmann, P. D.; MacLachlan, M. J. *Inorg. Chem.* **2011**, *50*, 2957–2965.
(25) (a) Dalla Cort, A.; De Bernardin, P.; Forte, G.; Mihan, Y. F. *Chem. Soc. Rev.* **2010**, *39*, 3863–3874. (b) Cano, M.; Rodríguez, L.; Lima, J. C.; Pina, F.; Dalla Cort, A.; Pasquini, C.; Schiaffino, L. *Inorg. Chem.* **2009**, *48*, 6229–6235. (c) Germain, M. E.; Vargo, T. R.; McClure, B. A.; Rack, J. J.; Van Patten, P. G.; Odoi, M.; Knapp, M. J. *Inorg. Chem.* **2008**, *47*, 6203–6211. (d) Wezenberg, S. J.; Escudero-Adán, E. C.; Benet-Bechholz, J.; Kleij, A. W. *Org. Lett.* **2008**, *10*, 3311–3314. (e) Germain, M. E.; Vargo, T. R.; Khalifah, P. G.; Knapp, M. J. *Inorg. Chem.* **2007**, *46*, 4422–4429. (f) Dalla Cort, A.; Mandolini, L.; Pasquini, C.; Rissanen, K.; Russo, L.; Schiaffino, L. *New J. Chem* **2007**, *31*, 1633–1638.
(26) (a) Decortes, A.; Kleij, A. W. *ChemCatChem* **2011**, *3*, 831–834. (b) Decortes, A.; Belmonte, M. M.; Benet-Buchholz, J.; Kleij, A. W. *Chem. Commun.* **2010**, *46*, 4580–4582. (c) Flapper, J.; Reek, J. N. H. *Angew. Chem., Int. Ed.* **2007**, *46*, 8590–8592. (d) Kuil, M.; Goudriaan, P. E.; Kleij, A. W.; Tooke, D. M.; Spek, A. L.; van Leeuwen, P. W. N. M.; Reek, J. N. H. *Dalton Trans.* **2007**, 2311–2320. (e) Kuil, M.; Goudriaan, P. E.; van Leeuwen, P. W. N. M.; Reek, J. N. H. *Chem. Commun.* **2006**, 4679–4681.
(27) Reviews: (a) Kleij, A. W. *Dalton Trans.* **2009**, 4635–4639. (b) Kleij, A. W. *Chem.—Eur. J.* **2008**, *14*, 10520–10529. (c) Wezenberg, S. J.; Kleij, A. W. *Angew. Chem., Int. Ed.* **2008**, *47*, 2354–2364.
(28) Recent literature: (a) Salassa, G.; Castilla, A. M.; Kleij, A. W. *Dalton Trans.* **2011**, *40*, 5236–5243. (b) Hui, J. K.-H.; MacLachlan, M. J. *Dalton Trans.* **2010**, *39*, 7310–7319. (c) Hui, J. K.-H.; Yu, Z.; Mirfakhrai, T.; MacLachlan, M. J. *Chem.—Eur. J.* **2009**, *15*, 13456–13465. (d) Wezenberg, S. J.; Escudero-Adán, E. C.; Benet-Buchholz, J.; Kleij, A. W. *Chem.—Eur. J.* **2009**, *15*, 5695–5700. (e) Jung, S.; Oh, M. *Angew. Chem., Int. Ed.* **2008**, *47*, 2049–2051. (f) Wezenberg, S. J.; Escudero-Adán, E. C.; Benet-Buchholz, J.; Kleij, A. W. *Inorg. Chem.* **2008**, *47*, 2925–2927. (g) Hui, J. K.-H.; Yu, Z.; MacLachlan, M. J. *Angew. Chem., Int. Ed.* **2007**, *46*, 7980–7983. (h) Kleij, A. W.; Kuil, M.; Tooke, D. M.; Lutz, M.; Spek, A. L.; Reek, J. N. H. *Chem.—Eur. J.* **2005**, *11*, 4743–4750. (i) Ma, C. T. L.; MacLachlan, M. J. *Angew. Chem., Int. Ed.* **2005**, *44*, 4178–4182.
(29) (a) Gallant, A. J.; Chong, J. H.; MacLachlan, M. J. *Inorg. Chem.* **2006**, *45*, 5248–5250. (b) Nabeshima, T.; Miyazaki, H.; Iwasaki, A.; Akine, S.; Saiki, T.; Ikeda, C.; Sato, S. *Chem. Lett.* **2006**, *35*, 1070–1071.
(30) (a) Ohshima, T.; Iwasaki, T.; Maegawa, Y.; Yoshiyama, A.; Mashima, K. *J. Am. Chem. Soc.* **2008**, *130*, 2944–2945. (b) Transesterification study: Iwasaki, T.; Maegawa, Y.; Hayashi, Y.; Ohshima, T.; Mashima, K. *J. Org. Chem.* **2008**, *73*, 5147–5150.
(31) Yaghi, O. M.; O'Keeffe, M.; Ockwig, N. W.; Chae, H. K.; Eddaoudi, M.; Kim, J. *Nature* **2003**, *423*, 705–714.
(32) (a) Yamamura, M.; Miyazaki, H.; Akine, S.; Nabeshima, T. *Inorg. Chem.* **2011**, *50*, 5315–5317. (b) Frischmann, P. D.; Gallant, A. J.; Chong, J. H.; MacLachlan, M. J. *Inorg. Chem.* **2008**, *47*, 101–112.
(33) Mezei, G.; Zaleski, C. M.; Pecoraro, V. L. *Chem. Rev.* **2007**, *107*, 4933–5003.
(34) Yamamura, M.; Sasaki, M.; Kyotani, M.; Orita, H.; Nabeshima, T. *Chem.—Eur. J.* **2010**, *16*, 10638–10643.
(35) *SIR1997*: Altomare, A.; Burla, M. C.; Camalli, M.; Cascarano, G. L.; Giacovazzo, C.; Guagliardi, A.; Moliterni, A. G. G.; Polidori, G.; Spagna, R. *J. Appl. Crystallogr.* **1999**, *32*, 115–119.
(36) Sheldrick, G. M. *SHELXL-97*; University of Göttingen: Göttingen, Germany, 1997.
(37) *SQUEEZE*: van der Sluis, P.; Spek, A. L. *Acta Crystallogr., Sect. A* **1990**, *46*, 194–201.
(38) Horman, I.; Dreux, B. *Helv. Chim. Acta* **1984**, *67*, 754–764.
(39) Frisch, M. J.; Trucks, G. W.; Schlegel, H. B.; Scuseria, G. E.; Robb, M. A.; Cheeseman, J. R.; Montgomery, Jr., J. A.; Vreven, T.; Kudin, K. N.; Burant, J. C.; Millam, J. M.; Iyengar, S. S.; Tomasi, J.; Barone, V.; Mennucci, B.; Cossi, M.; Scalmani, G.; Rega, N.; Petersson, G. A.; Nakatsuji, H.; Hada, M.; Ehara, M.; Toyota, K.; Fukuda, R.; Hasegawa, J.; Ishida, M.; Nakajima, T.; Honda, Y.; Kitao, O.; Nakai, H.; Klene, M.; Li, X.; Knox, J. E.; Hratchian, H. P.; Cross, J. B.; Bakken, V.; Adamo, C.; Jaramillo, J.; Gomperts, R.; Stratmann, R. E.; Yazyev, O.; Austin, A. J.; Cammi, R.; Pomelli, C.; Ochterski, J. W.; Ayala, P. Y.; Morokuma, K.; Voth, G. A.; Salvador, P.; Dannenberg, J. J.; Zakrzewski, V. G.; Dapprich, S.; Daniels, A. D.; Strain, M. C.; Farkas, O.; Malick, D. K.; Rabuck, A. D.; Raghavachari, K.; Foresman, J. B.; Ortiz, J. V.; Cui, Q.; Baboul, A. G.; Clifford, S.; Cioslowski, J.; Stefanov, B. B.; Liu, G.; Liashenko, A.; Piskorz, P.; Komaromi, I.; Martin, R. L.; Fox, D. J.; Keith, T.; Al-Laham, M. A.; Peng, C. Y.; Nanayakkara, A.; Challacombe, M.; Gill, P. M. W.; Johnson, B.; Chen, W.; Wong, M. W.; Gonzalez, C.; Pople, J. A. *Gaussian 03*, Revision D.02; Gaussian, Inc.: Wallingford, CT, 2004.
(40) Perdew, J. P.; Burke, K.; Ernzerhof, M. *Phys. Rev. Lett.* **1996**, *77*, 3865–3868.
(41) Schmider, H. L.; Becke, A. D. *J. Chem. Phys.* **1998**, *108*, 9624–9631.
(42) Adamo, C.; Barone, V. *J. Chem. Phys.* **1999**, *110*, 6158–6170.
(43) (a) Binkley, J. S.; Pople, J. A.; Hehre, W. J. *J. Am. Chem. Soc.* **1980**, *102*, 939–947. (b) Gordon, M. S.; Binkley, J. S.; Pople, J. A.; Pietro, W. J.; Hehre, W. J. *J. Am. Chem. Soc.* **1982**, *104*, 2797–2803. (c) Pietro, W. J.; Francl, M. M.; Hehre, W. J.; DeFrees, D. J.; Pople, J. A.; Binkley, J. S. *J. Am. Chem. Soc.* **1982**, *104*, 5039–5048. (d) Dobbs, K. D.; Hehre, W. J. *J. Comput. Chem.* **1986**, *7*, 359–378. (e) Dobbs, K. D.; Hehre, W. J. *J. Comput. Chem.* **1987**, *8*, 861–879. (f) Dobbs, K. D.; Hehre, W. J. *J. Comput. Chem.* **1987**, *8*, 880–893.
(44) Dunning, T. H., Jr.; Hay, P. J. In *Modern Theoretical Chemistry*; Schaefer, H. F., III, Ed.; Plenum: New York, 1976; Vol. 3, pp 1–28.
(45) Nicklass, A.; Dolg, M.; Stoll, H.; Preuss, H. *J. Chem. Phys.* **1995**, *102*, 8942–8952 , and references therein.
(46) Zhao, Y.; Truhlar, D. G. *Theor. Chem. Acc.* **2008**, *120*, 215–241.

(47) Boys, S. F.; Bernardi, F. *Mol. Phys.* **1970**, *19*, 553−566.
(48) Simon, S.; Duran, M.; Dannenberg, J. J. *J. Chem. Phys.* **1996**, *105*, 11024−11031.
(49) (a) Casida, M. E. Time dependent density functional response theory for molecules. In *Recent Advances in Density Functional Methods, Pt.1*; Chong, D. P., Ed.; World Scientific: Singapore, 1995; Vol. *1*, p 155; (b) Casida, M. E.; Jamorski, C.; Casida, K. C.; Salahub, D. R. J. *Chem. Phys.* **1998**, *108*, 4439−4449.
(50) Flückiger, P.; Lüthi, H. P.; Portmann, S.; Weber, J. *Molekel 4.3*; Swiss Center for Scientific Computing: Manno, Switzerland, 2000−2002; *MOLEKEL*: An Interactive Molecular Graphic Tool: Portmann, S.; Lüthi, H. P. *Chimia* **2000**, *54*, 766.
(51) See single-crystal X-ray diffraction section for experimental details.
(52) Mecozzi, S.; Rebek, J. Jr. *Chem.—Eur. J.* **1998**, *4*, 1016−1022.
(53) (a) Fairchild, R. M.; Holman, K. T. *J. Am. Chem. Soc.* **2005**, *127*, 16364−16365. (b) McKinlay, R. M.; Thallapally, P. K.; Cave, G. W. V.; Atwood, J. L. *Angew. Chem., Int. Ed.* **2005**, *44*, 5733−5736.
(54) See the Supporting Information of ref 23a.
(55) Cram, D. J.; Choi, H. J.; Bryant, J. A.; Knobler, C. B. *J. Am. Chem. Soc.* **1992**, *114*, 7748−7765.
(56) Kang, J.; Rebek, J. Jr. *Nature* **1996**, *382*, 239−241.
(57) Liu, S.; Gibb, B. C. *Chem. Commun.* **2008**, 3709−3716.
(58) Ben-Naim, A. *Molecular Theory of Solutions*; Oxford: New York, 2006.
(59) Ben-Naim, A. *Solvation Thermodynamics*; Plenum: New York, 1987.
(60) The values are: ΔH°_{solv} = −28.02, −29.53, −32.53, −36.60, and −41.13 kJ mol^{-1} and ΔS°_{solv} = −40.00, −40.29, −45.19, −50.29, and −56.90 J mol^{-1} K^{-1} for CH_2Cl_2, $CHCl_3$, benzene, toluene, and *p*-xylene, respectively.
(61) Experimentally measured ΔH°_{dim} and ΔS°_{dim} are equivalent to ΔH_{sol}^{dim} and ΔS_{sol}^{dim}, respectively.
(62) This convention is adopted to avoid confusion later in the derivation regarding the phase: solution or gas.
(63) (a) Pierotti, R. A. *J. Phys. Chem.* **1965**, *69*, 281−288. (b) Pierotti, R. A. *J. Phys. Chem.* **1963**, *67*, 1840−1845. (c) Reis, H.; Frisch, H. I.; Lebowitz, J. L. *J. Chem. Phys.* **1960**, *32*, 119−124. (d) Tomasi, J.; Mennucci, B.; Cammi, R. *Chem. Rev.* **2005**, *105*, 2999−3094.
(64) The value of the ratio ($B\underline{S}_mB/B\underline{S}_n$) between the two solvent cavity surfaces ($B\underline{S}_mB$ and $B\underline{S}_n$, respectively) and between their volumes computed according to the GePol algorithm[63] are 1.936 and 1.932, respectively.
(65) Pascual-Ahuir, J. L.; Silla, E.; Tuñón, I. *J. Comput. Chem.* **1994**, *15*, 1127−1138.
(66) Though $\Delta S^{(gas\rightarrow solv)}_{(relax)}$ cannot be excluded in principle, the entropy effects due to geometry reorganization from the gas phase to solution will be minimal compared to the entropy change due to immobilization of the two moieties when the dimer is formed. Therefore, it has been excluded from the analysis.
(67) According to our thermodynamic model, k_H and k_S should be the same.
(68) See Supporting Information, Figure 13 for a picture of one benzene molecule inside the bowl in a geometry that is compatible with a complex $B\underline{S}B$ as obtained by SDD/D95(d)/M06 level of theory.
(69) There is possibly a further assumption if inside the capsule or the monomeric bowl there is more than one molecule of solvent as guest. In this case we must also assume that the interaction enthalpy of the two molecules with the bowl is the same as a single molecule was inside.
(70) This value is the interaction enthalpy of the two bowls in the gas phase at the distance that they have in solution and should not be confused with the "real" interaction enthalpy of the two bowls in the gas phase at their equilibrium distance. The equilibrium distance in bulk solvent will likely be different than in the gas phase.
(71) (a) Hains, A. W.; Liang, Z.; Woodhouse, M. A.; Gregg, B. A. *Chem. Rev.* **2010**, *110*, 6689−6735. (b) Bottari, G.; de la Torre, G.; Guldi, D. M.; Torres, T. *Chem. Rev.* **2010**, *110*, 6768−6816. (c) Anthony, J. E.; Facchetti, A.; Heeney, M.; Marder, S. R.; Zhan, X. *Adv. Mater.* **2010**, *22*, 3876−3892.
(72) Yanagisawa, M.; Tashiro, K.; Yamasaki, M.; Aida, T. *J. Am. Chem. Soc.* **2007**, *129*, 11912−11913. For a review on host−guest fullerene interactions: Pérez, E. M.; Martín, N. *Pure Appl. Chem.* **2010**, *82*, 523−533.
(73) (a) Huerta, E.; Metselaar, G. A.; Fragoso, A.; Santos, E.; Bo, C.; de Mendoza, J. *Angew. Chem., Int. Ed.* **2007**, *46*, 202−205. (b) Huerta, E.; Cequier, E.; de Mendoza, J. *Chem. Commun.* **2007**, 5016−5018.
(74) Fernández, G.; Pérez, E. M.; Sánchez, L.; Martín, N. *Angew. Chem., Int. Ed.* **2008**, *47*, 1094−1097.
(75) (a) Grimm, B.; Isla, H.; Pérez, E. M.; Martín, N.; Guldi, D. M. *Chem. Commun.* **2011**, *47*, 7449−7451. (b) Grimm, B.; Santos, J.; Illescas, B. M.; Muñoz, A.; Guldi, D. M.; Martín, N. *J. Am. Chem. Soc.* **2010**, *132*, 17387−17389. (c) Gayathri, S. S.; Wielopolski, M.; Pérez, E. M.; Fernández, G.; Sánchez, L.; Viruela, R.; Ortí, E.; Guldi, D. M.; Martín, N. *Angew. Chem., Int. Ed.* **2009**, *48*, 815−819.